Journal of Magnetic Resonance **139,** 287–301 (1999)
Article ID jmre.1999.1784, available online at http://www.idealibrary.com on IDEAL®

Heteronuclear Double-Quantum MAS NMR Spectroscopy in Dipolar Solids

Kay Saalwächter, Robert Graf, Dan E. Demco,* and Hans W. Spiess[1]

*Max-Planck-Institut für Polymerforschung, Postfach 3148, D-55021 Mainz, Germany; and *Lehrstuhl für Makromolekulare Chemie, RWTH, Worringerweg 1, D-52074 Aachen, Germany*

Received December 1, 1998; revised April 2, 1999

A new pulse sequence for high-resolution solid-state heteronuclear double-quantum MAS NMR spectroscopy of dipolar-coupled spin-$\frac{1}{2}$ nuclei is introduced. It is based on the five-pulse sequence known from solution-state NMR, which is here applied synchronously to both spin species. The heteronuclear double-quantum (HeDQ) spinning-sideband patterns produced by this experiment are shown to be sensitive to the heteronuclear distance, as well as the relative orientations of the chemical-shift and dipolar tensors. In particular, it is shown that the HeDQ patterns exhibit an enhanced sensitivity to the chemical shielding tensors as compared with the single-quantum spinning-sideband patterns. The detection of HeDQ patterns via the I and S spins is discussed. The isolated ^{13}C–^{1}H spin pair in deuterated ammonium formate with ^{13}C in natural abundance was chosen as a model system, and the perturbing influence of dipolar couplings to surrounding protons on the ^{13}C–^{1}H DQ coherence is discussed. The pulse sequence can also be used as a heteronuclear double-quantum filter, hence providing information about heteronuclear couplings, and thus allowing the differentiation of quaternary and CH_n bonded carbons. The elucidation of ^{13}C–^{1}H dipolar proximities is presented for a sample of bisphenol A polycarbonate with ^{13}C in natural abundance, recorded with a broadband version of the synchronized five-pulse sequence. © 1999 Academic Press

Key Words: **double-quantum spectroscopy; heteronuclear dipolar correlation; CSA/dipolar tensor correlation; spinning-sideband patterns; magic-angle spinning.**

INTRODUCTION

Multiple-quantum (MQ) nuclear magnetic resonance (NMR) spectroscopy is a valuable tool for the identification and characterization of spin systems in solution (*1–4*), where MQ methods have proved to be particularly useful for both spectral simplification and the analysis of molecular motion. In such solution-state applications, the excitation of MQ coherences between like spins is achieved by utilizing the *J* coupling between the nuclei in a two-dimensional experiment, which in the simplest version consists of three pulses (*1*). An extension to this sequence to include a *z* filter (*5*), henceforth referred to as the five-pulse sequence, exhibits some experimental advantages, but is based on the same principles. MQ spectroscopy is not restricted to homonuclear spin systems; for example, *heteronuclear* multiple-quantum correlation (HMQC) experiments involving two different spin species correlate the chemical shifts of spins within one molecule via the heteronuclear *J* coupling (*6, 7*).

In the solid state, the absence of isotropic molecular tumbling means that anisotropic interactions, namely, for spin-$\frac{1}{2}$ nuclei, strong dipolar interactions, and the chemical-shift anisotropy (CSA), must be considered. The broadenings associated with these anisotropic interactions complicate the experiments and substantially limit the spectral resolution. Nevertheless, in recent years, there has been a sustained effort by different research groups in this field, and both homonuclear ^{1}H–^{1}H (*8–13*), ^{13}C–^{13}C (*14–17*), and ^{31}P–^{31}P (*18, 19*) and heteronuclear ^{13}C–^{1}H (*20*) and ^{13}C–^{15}N (*21*) high-resolution solid-state MQ spectra have been measured. By harnessing the inherent information content of the anisotropic dipolar and CSA interactions, much information about both structure and dynamics in solids can be obtained. For example, homonuclear high-resolution DQ measurements to probe proximities have already found successful applications in structural determination studies of hydrogen-bonded systems (*13*) and crystalline as well as disordered ^{13}P–^{31}P phosphate systems (*18, 19*). Moreover, by evaluating residual dipolar couplings in polymer melts and elastomers, MQ NMR was shown to probe polymer dynamics on time- and lengthscales not accessible by other methods (*10, 11*). Also, MQ methods can act as a dipolar filer for rigid domains in semicrystalline polymers (*14*). MQ spectroscopy has furthermore opened up the possibility of determining torsion angles in polymeric (*15, 16*) and biological (*17, 21*) systems, this being an important step toward structure determination of increasingly complex molecules in the solid state.

These solid-state methods differ from their solution-state analogues in that they employ the dipolar coupling rather than the comparably weak *J* coupling to excite the MQ coherences. Additionally, in most of the above examples, high resolution is achieved by applying fast magic-angle spinning (MAS), and such methods are henceforth referred to as MQ MAS NMR

[1] To whom correspondence should be addressed.

1090-7807/99 $30.00

spectroscopy. Under MAS, there are two different methods for the excitation and reconversion of MQ coherences. First, the three- or five-pulse solution-state sequences can be used. The averaging of the dipolar coupling by MAS means that this approach is however limited to excitation times of half a rotor period, $\tau_R/2$, and is thus applicable to only strong dipolar interactions or slow MAS spinning frequencies (*9*). On account of the analogy to the solution-state method, MQ excitation utilizing the three- or five-pulse sequence will thus be referred to as "quasi-static." Alternatively, so-called dipolar recoupling methods such as Back-to-Back (*14*) or C7 (*16*, and references therein) must be used.

An important feature and a valuable source of information in MQ MAS NMR spectroscopy is the presence of spinning-sideband patterns in the MQ dimension of the spectra (*8, 9, 12, 14, 16, 21*). These patterns originate from two distinct mechanisms (*12*), first, rotor encoding of the reconversion Hamiltonian, and second, evolution of the excited MQ coherences under local interactions, for example, dipolar couplings to other spins. Only the first mechanism is present in total spin coherence spectroscopy (i.e., where the MQ coherence corresponds to the highest excitable coherence). The simplest such example is represented by double-quantum (DQ) NMR of isolated spin-$\frac{1}{2}$ pairs. The DQ spinning-sideband patterns obtained in this case have been investigated for inorganic and organic solids with well-localized homonuclear dipolar interactions (*9, 14*). Additionally, it has been shown both theoretically and experimentally that only odd-order sidebands are expected for an isolated spin pair when using a quasi-static excitation method with $\tau = \tau_R/2$ (*12*).

In this paper, we present a new scheme for high-resolution heteronuclear DQ (HeDQ) spectroscopy of dipolar-coupled ^{13}C–^{1}H spin pairs in natural abundance, based on quasi-static excitation under MAS. We show that HeDQ spinning-sideband patterns can be obtained by the simple application of a synchronized five-pulse sequence (referred to as SYNCHRON4, since four of the five pulses, representing DQ excitation and reconversion, are applied synchronously on both channels). Such patterns are dependent on both heteronuclear dipolar couplings, and hence internuclear distances, and the relative orientation of the CSA tensor relative to the heteronuclear dipolar tensor.

Methods for obtaining similar information were developed much earlier, a large class of those being referred to as separated local field (SLF) NMR experiments (*1*), where the application of homo- and heteronuclear decoupling of the abundant spins, together with optional refocusing pulses on the rare spin channel, in the two dimensions of a two-dimensional (2D) double-resonance experiment allows the correlation or separation of different isotropic and anisotropic interactions. The determination of dipolar coupling constants and the relative orientations of the dipolar and CSA tensors in single crystals (*22*) as well as in powdered samples (*23–25*) has been reported. For an overview of these and other methods for the determination of distances via dipolar couplings under MAS, such as REDOR (*r*otational-*e*cho *do*uble *r*esonance, (*26*)) and rotational resonance, see Ref. (*27*). Recently, the SLF method has been extended to experiments involving homonuclear DQ instead of SQ coherences in the first dimension of the experiment. Using such an approach, torsional angles could be determined by Schmidt-Rohr for the static case (*15*), and by Levitt and co-workers (*16*) under MAS. Torsion angle measurements in labeled amino acids using the SLF scheme involving HeDQ coherences, excited by an HMQC sequence with REDOR-type recoupling under MAS, have also been published by Hong *et al.* (*21*).

Although the comparably simple SYNCHRON4 experiment is not specifically designed to measure relative tensor orientations, we show a dependence of the HeDQ dipolar spinning-sideband patterns on the orientation of the chemical shielding tensor. This topic will be discussed under Theory, where we give an analytical treatment for so-obtained spinning-sideband patterns. The arguments will be supported by numerical simulations as well as experimental measurements on a model system containing an isolated ^{1}H–^{13}C spin pair, in our case deuterated ammonium formate. We emphasize the fact that the technique is suitable for measurements of ^{13}C in *natural abundance.*

As a more qualitative approach, in the last section of the paper the SYNCHRON4 experiment is shown to be useful for providing information about heteronuclear dipolar proximities, allowing spectral editing for peak assignments. The investigation of *through-bond* connectivities in the solid state using the *J* couplings in an HMQC experiment has been reported previously by Franke *et al.* (*28*), but, due to long MQ excitation times, these experiments suffer from low *S*/*N*. From our experiment, relative dipolar *through-space* ^{13}C–^{1}H proximites can easily be derived from a 2D HeDQ spectrum or even from simple HeDQ-filtered measurements. This is demonstrated for a sample of bisphenol A polycarbonate, again measured with ^{13}C in *natural abundance.* To achieve DQ excitation independent of the spectral offset, a broadband version of the SYNCHRON4 sequence is presented. The effect of molecular motion on the HeDQ spinning sidebands is also discussed.

THEORY

As a starting point, we consider an isolated rigid heteronuclear spin-$\frac{1}{2}$ pair (IS), where the two nuclear species I and S have magnetogyric ratios γ_I and γ_S, respectively, and are coupled by dipolar (D) interaction. The influence of the chemical-shift interaction is considered for both nuclei.

Heteronuclear double-quantum coherences are excited under magic-angle sample spinning by the SYNCHRON4 pulse sequence presented in Fig. 1. The full 2D experiment can be subdivided into five periods. The preparation period may consist, as shown in Fig. 1, of a Hartmann–Hahn cross-polarization (CP) pulse sequence and subsequent 90° flip-back pulses

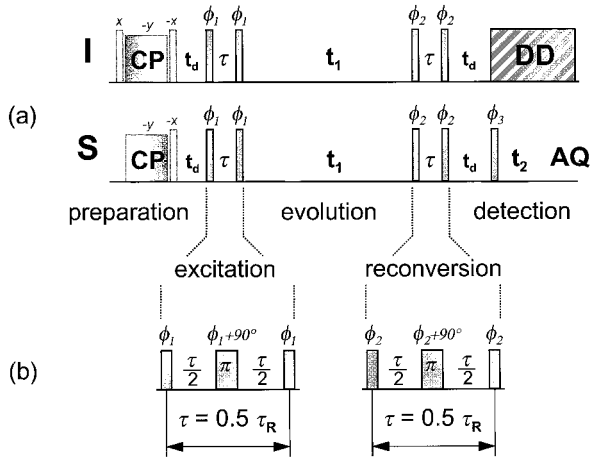

FIG. 1. Pulse schemes for heteronuclear double-quantum spectroscopy under fast MAS. Narrow bars correspond to 90° pulses. In (a), the different stages of the experiment are identified. The preparation period usually consists of a conventional CP sequence, storing the magnetization on both channels along the z direction to create initial I- *and* S-spin polarization. The evolution interval during excitation/reconversion, τ, must be set equal to half a rotor period to obtain properly phased spectra. For the selection of pure DQ evolution during t_1, the phases of all pulses belonging to the respective periods are cycled together as a group, following the phase cycling procedure described in the text. To achieve an offset-independent broadband excitation of DQ coherences, π pulses must be inserted into the excitation and reconversion intervals, respectively (b).

on both channels to generate z polarization for both spin species. Alternatives are first to leave out the proton flip-back pulse, thus allowing the proton magnetization to dephase, or second to miss out the CP step and additionally destroy any residual S-spin polarization by applying saturation pulses, such that only initial S- or I-spin polarization remains. The effects of these variations will be discussed below.

The first two 90° pulse pairs with the same phase, ϕ_1, separated by the time τ, represent the excitation period. The detection of multiple-quantum coherences alone can be achieved by a standard phase cycle of these pulses, as described under Experimental. The 90° pulse pair and the subsequent second delay τ, which follow the MQ evolution period of variable duration t_1, represent the reconversion period, while the last 90° pulse pair and the purging period t_d act as a z filter to suppress unwanted signal contributions. In comparison to the classical three-pulse sequence, the inclusion of a z filter not only gives cleaner spectra, but is in our case *essential* because of CSA evolution during excitation/reconversion. Without a z filter, it is not possible to achieve correct amplitude modulation of the signal at $t_2 = 0$ with respect to the evolution in t_1, resulting in phase errors in the final 2D spectrum. The incomplete evolution through all orientations of the CSA tensor for $\tau_R/2$ will always lead to some contribution to the imaginary part of the signal at $t_2 = 0$, which is supposed to be zero for pure amplitude modulation. This problem is easily avoided by applying the z filter.

The first four pulses of the original five-pulse sequence are synchronously applied to both radiofrequency channels. The fifth pulse is a read-out pulse and can in principle be applied to either of the two spin species. For optimum spectral resolution, we chose to acquire the rare spin (S = ^{13}C) signal.

In order to handle the spectral width of ^{13}C chemical shifts, the pulse sequence to be used in the case of off-resonance excitation is slightly more complicated (Fig. 1b). Evolution of the spin system due to *isotropic* chemical shifts is refocused by applying π pulses during excitation and reconversion. This is important for samples with more than one carbon signal, since due to the large chemical-shift dispersion of ^{13}C, the antiphase magnetizations from signals at the edges of the spectrum would have evolved almost completely out of phase with respect to the last pulse of the excitation/reconversion periods, so that virtually no DQ signal would be created. By means of refocusing, uniform excitation efficiency is thus achieved for the whole spectral range, but at the expense of an interference of the π pulses with the chemical-shift anisotropy. This will be dealt with under Experimental. For the sake of clarity of the calculations, the compensation is not included in the analytical treatment of the sequence.

Rotor-Modulated Spin Hamiltonians

The secular approximation of the heteronuclear dipolar Hamiltonian (denoted by $^{(0)}$), modulated by MAS at a spinning frequency ω_R, is given by

$$H^{(0)}_{D,IS}(t) = 2d_{IS}(t)I_zS_z, \qquad [1]$$

where we define

$$d_{IS}(t) \equiv \sum_{m=-2}^{2} -2D_{IS}d^{(2)}_{-m,0}(\beta_M)\,D^{(2)}_{0,-m}(\Omega_{P_DR}) \times \exp\{im\omega_R t\}I_zS_z. \qquad [2]$$

I and **S** represent the spin operators of the dipolar-coupled nuclei, and Ω_{P_DR} denotes the set of Euler angles (α_D^{IS}, β_D^{IS}, γ_D^{IS}) relating the principal axes system (PAS) of the dipolar coupling tensor (P_D) of the heteronuclear IS spin-$\frac{1}{2}$ pair to the rotor (R) reference frame. Thus, powder averaging has to be performed over Ω_{P_DR}. As long as chemical-shift anisotropy is neglected, the angle α_D^{IS} is arbitrary and can be omitted from the averaging procedure. In addition, $\beta_M = \arccos(1/\sqrt{3}) = 54.7^0$ denotes the magic angle between the rotor axis and the static magnetic field. The Wigner rotation matrices $D^{(2)}_{m,m'}(\alpha, \beta, \gamma) = \exp(-im\alpha)d^{(2)}_{m,m'}(\beta)\exp(-im'\gamma)$ follow the conventions of Refs. (*29, 30*). The heteronuclear dipolar coupling constant $D_{IS} = (\mu_0/4\pi)\gamma_I\gamma_S\hbar/r^3_{IS}$ depends on the internuclear distance r_{IS} and on the magnetogyric ratios γ_j of the nuclei involved.

The computation of the spin propagators describing the free evolution of the spin system under MAS requires the spatial

part of the rotor-modulated dipolar Hamiltonian $d_{\mathrm{IS}}(t)$ to be integrated over time,

$$H^{(0)}_{\mathrm{D,IS}}(t'', t') = \int_{t'}^{t''} H^{(0)}_{\mathrm{D,IS}}(t)dt = \int_{t'}^{t''} 2d_{\mathrm{IS}}(t)dtI_zS_z \equiv 2d_{\mathrm{IS}}(t''; t')I_zS_z, \quad [3]$$

where

$$d_{\mathrm{IS}}(t''; t') = \frac{D_{\mathrm{IS}}}{2\omega_{\mathrm{R}}}\{\sqrt{2}\sin(2\beta^{\mathrm{IS}}_{\mathrm{D}})[\sin(\omega_{\mathrm{R}}t'' + \gamma^{\mathrm{IS}}_{\mathrm{D}}) - \sin(\omega_{\mathrm{R}}t' + \gamma^{\mathrm{IS}}_{\mathrm{D}})] - \tfrac{1}{2}\sin^2(\beta^{\mathrm{IS}}_{\mathrm{D}})[\sin(2\omega_{\mathrm{R}}t'' + 2\gamma^{\mathrm{IS}}_{\mathrm{D}}) - \sin(2\omega_{\mathrm{R}}t' + 2\gamma^{\mathrm{IS}}_{\mathrm{D}})]\}. \quad [4]$$

To take into account chemical-shift effects, it must be remembered that the corresponding chemical-shift anisotropy PASs may differ from that of the dipolar tensor. The time-dependent chemical shielding Hamiltonians are then

$$H^{\mathrm{I}}_{\mathrm{CS}}(t) = -\omega_{0\mathrm{I}}\sigma^{\mathrm{I}}_{\mathrm{CS}}(t)I_z, \quad [5]$$

$$H^{\mathrm{S}}_{\mathrm{CS}}(t) = -\omega_{0\mathrm{S}}\sigma^{\mathrm{S}}_{\mathrm{CS}}(t)S_z, \quad [6]$$

where the space parts of the chemical-shift Hamiltonians are given by

$$\sigma^j_{\mathrm{CS}}(t) = \sigma^j_{\mathrm{iso}} - \frac{\delta_j}{\omega_{0j}}\sum_{\substack{m\neq 0\\ m=-2}}^{2}\sum_{n=-2}^{2}\left\{D^{(2)}_{0,n}(\Omega^j_{P_{\mathrm{CS}}P_{\mathrm{D}}})D^{(2)}_{n,-m}(\Omega^{\mathrm{IS}}_{P_{\mathrm{D}}\mathrm{R}}) - \frac{1}{\sqrt{6}}\eta_{\mathrm{I}}[D^{(2)}_{-2,n}(\Omega^j_{P_{\mathrm{CS}}P_{\mathrm{D}}})D^{(2)}_{n,-m}(\Omega^{\mathrm{IS}}_{P_{\mathrm{D}}\mathrm{R}}) + D^{(2)}_{2,n}(\Omega^j_{P_{\mathrm{CS}}P_{\mathrm{D}}})D^{(2)}_{n,-m}(\Omega^{\mathrm{IS}}_{P_{\mathrm{D}}\mathrm{R}})]\right\}d^{(2)}_{-m,0}(\beta_{\mathrm{M}})e^{im\omega_{\mathrm{R}}t}. \quad [7]$$

In the above expression j equals I or S, while $\omega_{0j}\sigma^j_{\mathrm{iso}}$ is the isotropic precession frequency, with $\sigma^j_{\mathrm{iso}} = 1/3(\sigma^j_x + \sigma^j_y + \sigma^j_z)$ representing the isotropic part of the CSA tensor and ω_{0j} denoting the Larmor frequency of the j spin species. The traceless symmetric part of the tensor in its principal axes system is characterized by the anisotropy parameter in frequency units, $\delta_j \equiv -\omega_{0j}(\sigma^j_z - \sigma^j_{\mathrm{iso}})$, and the asymmetry parameter $\eta \equiv (\sigma^j_y - \sigma^j_x)/\delta_j$ (*29*). The set of Euler angles describing the orientation of the chemical shielding tensors in the PAS of the heteronuclear dipolar tensor (i.e., the molecular frame) is denoted by $\Omega^j_{P_{\mathrm{CS}}P_{\mathrm{D}}}$, and the corresponding Euler angles are termed $(\alpha^j_{\mathrm{CS}}, \beta^j_{\mathrm{CS}}, \gamma^j_{\mathrm{CS}})$. Only $(\alpha^j_{\mathrm{CS}}, \beta^j_{\mathrm{CS}})$, then simply representing two polar angles, need to be considered if CSA is only effectively present for one of the two spins. This will be dealt with in the Appendix.

The time integrals of the chemical-shift Hamiltonians present in the spin propagators are then given by

$$H^{\mathrm{I}}_{\mathrm{CS}}(t'', t') = \int_{t'}^{t''} H^{\mathrm{I}}_{\mathrm{CS}}(t)dt = -\omega_{0\mathrm{I}}\int_{t'}^{t''}\sigma^{\mathrm{I}}_{\mathrm{CS}}(t)dtI_z \equiv -\omega_{0\mathrm{I}}\sigma^{\mathrm{I}}_{\mathrm{CS}}(t''; t')I_z, \quad [8]$$

and similarly

$$H^{\mathrm{S}}_{\mathrm{CS}}(t'', t') = -\omega_{0\mathrm{S}}\sigma^{\mathrm{S}}_{\mathrm{CS}}(t''; t')S_z, \quad [9]$$

where

$$\sigma^j_{\mathrm{CS}}(t''; t') = \frac{1}{\omega_{\mathrm{R}}}\left\{C^j_1(\sin(\gamma^{\mathrm{IS}}_{\mathrm{D}} + \omega_{\mathrm{R}}t'') - \sin(\gamma^{\mathrm{IS}}_{\mathrm{D}} + \omega_{\mathrm{R}}t')) + \frac{C^j_2}{2}(\sin(2\gamma^{\mathrm{IS}}_{\mathrm{D}} + 2\omega_{\mathrm{R}}t'') - \sin(2\gamma^{\mathrm{IS}}_{\mathrm{D}} + 2\omega_{\mathrm{R}}t')) - S^j_1(\cos(\gamma^{\mathrm{IS}}_{\mathrm{D}} + \omega_{\mathrm{R}}t'') - \cos(\gamma^{\mathrm{IS}}_{\mathrm{D}} + \omega_{\mathrm{R}}t')) - \frac{S^j_2}{2}(\cos(2\gamma^{\mathrm{IS}}_{\mathrm{D}} + 2\omega_{\mathrm{R}}t'') - \cos(2\gamma^{\mathrm{IS}}_{\mathrm{D}} + 2\omega_{\mathrm{R}}t'))\right\}. \quad [10]$$

The dependencies on the remaining angles and the tensor components reside in the coefficients $C^j_{1,2}$ and $S^j_{1,2}$. These coefficients depend on CSA/dipolar PAS orientations and CSA tensor components, and are given in the Appendix, where special cases and possible simplifications are discussed.

HeDQ Spinning-Sideband Patterns

The spin system response for the experiment in Fig. 1, based on synchronous radiofrequency excitation in heteronuclear spin systems, is calculated using density operator formalism (*1*). For the heteronuclear case, the ensemble of dipolar-coupled pairs behaves inhomogeneously; i.e., the dipolar Hamiltonians commute with themselves and with the chemical-shift Hamiltonians at each moment in time. Therefore, the spin evolution under these interactions can be evaluated independently.

At the end of the preparation period (see Fig. 1), the initial

density operator can be written in the high-temperature approximation as

$$\rho(0) \cong p_I I_z + p_S S_z, \qquad [11]$$

where p_I and p_S are factors describing the relative magnitude of the initial magnetizations. Depending on the preparation period of the experiment, these factors depend on the procedure used for cross-polarization (CP), its efficiency, or just represent the spin population in thermal equilibrium. For the case of normal CP, p_I and p_S depend on the orientation of each crystallite relative to the rotor axis, and thus distortions of the MQ spinning-sideband patterns could be expected. However, such distortions were not observed experimentally, and numerical density matrix simulations further showed that this possible source of error is not significant. The p_I factor can be set to zero if the I-spin transverse signal after cross-polarization is left to dephase, and is not stored in the z direction. Alternatively $p_I = p_{I,eq}$ and $p_S = 0$ for the case where the experiment is conducted in such a way that I spins are polarized and the S-spin signal is saturated at the beginning of the experiment.

The density operator at the end of the excitation period is given by

$$\rho(\tau) = P_x^I P_x^S E(\tau; 0) P_x^I P_x^S \rho(0) \times P_x^{S\,-1} P_x^{I\,-1} E(\tau; 0)^{-1} P_x^{S\,-1} P_x^{I\,-1}, \qquad [12]$$

which can be obtained from solving the Liouville–von Neumann equation. The propagators describing I and S $\pi/2$ radio-frequency pulses are $P_x^I = \exp(i\frac{\pi}{2}I_x)$ and $P_x^S = \exp(i\frac{\pi}{2}S_x)$, respectively, while the evolution propagator for the $(\tau; 0)$ time interval is

$$E(\tau; 0) = \exp\{-i2d_{IS}(\tau; 0) I_z S_z\} \exp\{i\omega_{0I}\sigma^I(\tau; 0) I_z\} \times \exp\{i\omega_{0S}\sigma^S(\tau; 0) S_z\}, \qquad [13]$$

where the notations introduced in Eqs. [3] and [8] are used to express the quantities present in the exponents. Using these propagators within straightforward product operator algebra (*31*), we obtain

$$\begin{aligned}\rho(\tau) = p_I\{&-I_z\cos[d_{IS}(\tau; 0)]\cos[\omega_{0I}\sigma^I_{CS}(\tau; 0)] \\ &- I_x\cos[d_{IS}(\tau; 0)]\sin[\omega_{0I}\sigma^I_{CS}(\tau; 0)] \\ &+ 2I_zS_y\sin[d_{IS}(\tau; 0)]\sin[\omega_{0I}\sigma^I_{CS}(\tau; 0)] \\ &- 2I_xS_y\sin[d_{IS}(\tau; 0)]\cos[\omega_{0I}\sigma^I_{CS}(\tau; 0)]\} \\ + p_S\{&-S_z\cos[d_{IS}(\tau; 0)]\cos[\omega_{0S}\sigma^S_{CS}(\tau; 0)] \\ &- S_x\cos[d_{IS}(\tau; 0)]\sin[\omega_{0S}\sigma^S_{CS}(\tau; 0)] \\ &+ 2S_zI_y\sin[d_{IS}(\tau; 0)]\sin[\omega_{0S}\sigma^S_{CS}(\tau; 0)] \\ &- 2S_xI_y\sin[d_{IS}(\tau; 0)]\cos[\omega_{0S}\sigma^S_{CS}(\tau; 0)]\}. \end{aligned} \qquad [14]$$

At the end of the excitation period, the spin modes present are longitudinal magnetization (I_z and S_z terms), single-quantum (SQ) coherences (I_x and S_x terms), antiphase magnetization (I_zS_y and S_zI_y terms), and heteronuclear zero-quantum (HeZQ) as well as HeDQ coherences (I_xS_y and S_xI_y terms). A phase cycle applied to the excitation or reconversion pulses allows us to distinguish and separate these spin modes with the exception of longitudinal magnetization and HeZQ. It is also evident from Eq. [14] that the MQ coherences (I_xS_y and S_xI_y), which can be detected on either channel, are encoded by the CS Hamiltonian during *excitation*, in a way which depends on the mode of preparation (represented by the coefficients p_I and p_S).

The HeDQ coherences are selected by the phase cycle and thus we only consider what happens to these coherences in the latter periods of the experiment. For an isolated IS spin pair, HeDQ coherences are total spin coherences, i.e., $[I_\pm S_\pm, H^{(0)}_{D,IS}(t)] = 0$, and consequently do not evolve under dipolar coupling. Nevertheless, *both* chemical-shift interactions modulate HeDQ coherences during the *evolution* period.

Sign discrimination of the DQ evolution during t_1 is experimentally achieved by shifting the reconversion phases by 45°. For the same value of t_1 and the two reconversion phase settings, the spectrum in the direct dimension will be modulated by the x and the y component of the DQ signal, respectively. Performing the 2D experiment this way, a hypercomplex dataset will result. It is also possible to increment the reconversion phases in steps of 45° for subsequent increments of t_1. This is the TPPI method, which is commonly used in single-quantum 2D experiments (*1, 29*). These considerations are based on the fact that the sensitivity of a DQ coherence to a phase shift $\Delta\phi$ of the excitation or reconversion pulses is twice that value in effect. To simplify calculations, the same effect is achieved by shifting the phases on only one channel by 90°. The normalized orthogonal signals detected in the t_1 dimension can then be calculated to be

$$S^j_x(t_1; t_2 = 0) \propto a \cdot b_x \cdot c, \qquad [15]$$

where

$$\begin{aligned} a &= \sin\{d_{IS}(\tau; 0)\}\{p_I\cos\{\omega_{0I}\sigma^I_{CS}(\tau; 0)\} + p_S\cos\{\omega_{0S}\sigma^S_{CS}(\tau; 0)\}\}, \\ b_x &= \cos\{\omega_{0I}\sigma^I_{CS}(t_1 + \tau; \tau) + \omega_{0S}\sigma^S_{CS}(t_1 + \tau; \tau)\}, \\ c &= \sin\{d_{IS}(\tau + t_1 + \tau; t_1 + \tau)\} \times \cos\{\omega_{0I}\sigma^j_{CS}(\tau + t_1 + \tau; t_1 + \tau)\}, \end{aligned}$$

and

$$S^j_y(t_1; t_2 = 0) \propto a \cdot b_y \cdot c, \qquad [16]$$

where

$$b_y = \sin\{\omega_{0I}\sigma^I_{CS}(t_1 + \tau; \tau) + \omega_{0S}\sigma^S_{CS}(t_1 + \tau; \tau)\},$$

where j denotes the detected spin species and therefore must be replaced by either I or S. In the case of powdered samples, an average of the above equations over the orientations Ω_{PDR} of the dipolar tensor must be performed.

The following conclusions can be drawn from the above results:

(i) The *heteronuclear dipolar coupling* only contributes to the spinning-sideband pattern on account of the *encoding in the reconversion period*, given by the t_1 dependence of d_{IS} in the coefficient c of Eqs. [15] and [16]. This reflects directly the total spin coherence character of HeDQ coherences excited in an isolated IS spin pair, with dipolar interactions of the DQ coherence to remote spins being neglected in the above derivation.

(ii) The *CSA interactions* encode the HeDQ patterns due to the rotor modulation during the *evolution* period (contributions b_x and b_y) as well as during the *excitation* (contribution a) and *reconversion* periods (contribution c). In comparison, the heteronuclear-encoded single-quantum signal, given by

$$S_x^j(t) = p_j \cos\{d_{IS}(t;\,0)\}\cos\{\omega_{0j}\sigma_{CS}^j(t;\,0)\} \qquad [17]$$

and

$$S_y^j(t) = -p_j \cos\{d_{IS}(t;\,0)\}\sin\{\omega_{0j}\sigma_{CS}^j(t;\,0)\}, \qquad [18]$$

exhibits only effects of *CSA* interactions corresponding to those of the *evolution* period. Thus, the additional chemical-shift evolution during *excitation* and *reconversion* gives an *enhanced* effect of the chemical-shift interaction on the double-quantum spinning-sideband patterns, depending on the coefficients p_I and p_S, which are under the control of the experimentalist.

(iii) Both I- and S-spin signals carry information about the relative orientation of the CS and heteronuclear dipolar tensors. This provides a basis for experiments to determine these angles using HeDQ coherences.

(iv) If the CSA tensor of one spin species has rather small components, as, for example, I = ^{1}H in the case of a ^{13}C–^{1}H pair, Eqs. [15] and [16] can be simplified by setting $\sigma_{CS}^I(t''; t') = 0$. Neglecting σ_{CS}^S as well will yield formulae which are, apart from the prefactor in the dipolar coupling constant d_{IS}, identical to those for the homonuclear case (*9*). This is obvious, because in both cases the mechanism of sideband generation is identical; the sidebands result only from the rotor encoding of the reconversion period.

(v) The above equations are general, describing the HeDQ spinning-sideband patterns recorded using different experimental preparation procedures. For instance, if after the cross-polarization process I → S the I-spin transverse magnetization is not stored along the z direction by a flip-back pulse and allowed to dephase, we can set $p_I = 0$ in Eqs. [15] and [16]. Furthermore, if presaturation pulses are applied to S spins instead of a CP and only the polarization of the I spins is used for the experiment, the HeDQ patterns can nevertheless be detected at both resonances and are described by Eqs. [15] and [16] with $p_S = 0$. Thus, the preparation period enables one to control which spin's CSA influences the pattern during *excitation.* Moreover, the HeDQ pattern can be detected at both resonances, with the difference that the *CSA influence* on the pattern during *reconversion* is only that of the *detected* nucleus.

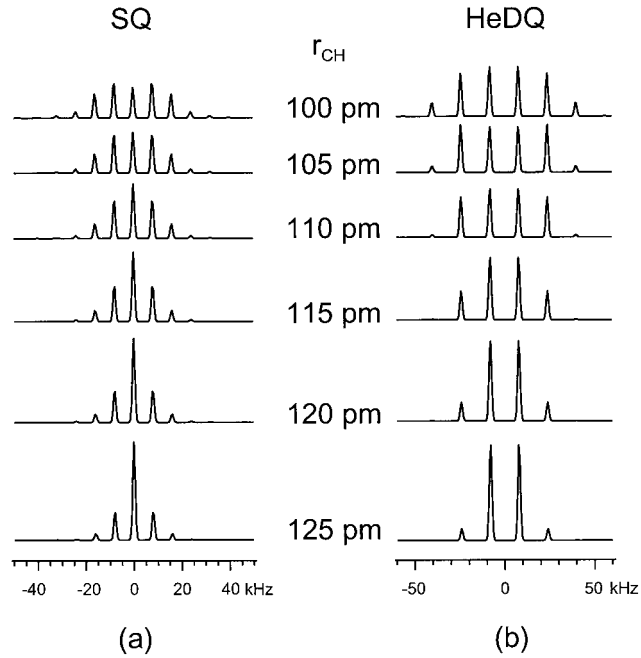

FIG. 2. Calculated dipolar (a) ^{13}C SQ and (b) HeDQ spinning-sideband patterns for a ^{13}C–^{1}H spin pair at 8 kHz MAS. The spectra represent solutions of Eqs. [17] and [18] and [15] and [16], respectively, after powder averaging and Fourier transformation, and are plotted on the same vertical scale. CSA was neglected for these calculations.

Simulations

In Fig. 2, heteronuclear ^{13}C-detected dipolar-encoded single- and double-quantum spinning-sideband patterns are compared for a typical range of ^{13}C–^{1}H bond distances. The spectra were calculated by Fourier transformation of the time domain signals given by Eqs. [17] and [18] and [15] and [16], respectively. Powder averaging was performed using a set of 192 pairs of (β_D^{IS}, γ_D^{IS}) angles describing vector orientations evenly distributed on a sphere, as generated using the REPULSION method (*32*). For each orientation, the signal was averaged over 25 values for γ_D^{IS} between 0° and 360°, resulting in a total number of 4800 interaction tensor orientations. The chemical-shift anisotropy (CSA) was neglected in these calculations, and the spinning frequency was set equal to 8 kHz.

The HeDQ patterns for a heteronuclear spin-$\frac{1}{2}$ pair presented in Fig. 2b share many similarities with homonuclear spin-pair DQ patterns recorded using the three (or five)-pulse sequence (*9*). In both cases, the centerband is absent, with the sidebands at $\pm\nu_R$ being the most intense. Exclusively odd-order spinning sidebands without phase distorsions are present only for excitation/reconversion times $\tau = \tau_R/2$ (where τ_R is the rotor period). In the limit of very fast MAS, i.e., $\omega_R/D_{IS} \gg 1$, both types of DQ patterns are composed of mainly spinning sidebands of first order. These considerations also illustrate the restrictions of quasi-static excitation, i.e., being limited to only strong couplings (or slow MAS) and the missing freedom in excitation time. Thus, the study of DQ excitation dynamics and the measurement of weak couplings must be left to recoupling sequences. Variation of the spinning speed is a possible way of finding a suitable compromise between either distributing the intensity over too many sidebands or having too few sidebands, such that a fitting procedure for extracting the heteronuclear distance is no longer possible.

The sensitivity of SQ and HeDQ patterns to the variation of the distance is rather similar, although it should be noted that the *S*/*N* is smaller for heteronuclear DQ MAS spectra, especially where the nuclei involved have small gyromagnetic ratios. The advantages of HeDQ spectra will, however, become apparent when considering the influence of additional interactions on the DQ coherence, for example, CSA or dipolar couplings to remote spins.

If one of the two nuclei in question exhibits a CSA which is large with respect to the spinning speed, the patterns show a pronounced asymmetry. The patterns in Fig. 3 were calculated using the principal values of the formate tensor measured for calcium formate (*33*). For $\beta^j_{CS} = 0$, the orientation of the CSA tensor is such that the least shielded direction (σ_z) points along the dipolar axis; this is what would be expected from chemical intuition, if possible packing effects are ignored. The asymmetry of the pattern is more pronounced in the HeDQ case, mostly due to the fact that there is no strong centerband intensity as in the SQ case. It should be noted that the influence of CSA additionally leads to *the appearance of weak even-order sidebands.* Moreover, the patterns are dependent on the relative orientation of the dipolar and the chemical-shift tensor. This effect can serve as a basis for new experiments for the determination of these angles, which have been measured before in single-crystal studies (*33*) based on X-ray diffraction results, or using static 2D SLF spectroscopy (*23*). In addition, the relative orientation of the heteronuclear dipolar tensor and the chemical shielding tensors can be also measured using SQ spinning-sideband patterns (*27*, and references therein). As noted under Theory, the encoding of the chemical-shift interaction on the HeDQ spinning-sideband patterns is present during the excitation, evolution, and reconversion periods as is evident in Eqs. [15] and [16]. Hence, the effect of CSA is *enhanced* in HeDQ patterns compared with the SQ patterns. Naturally, the possible accuracy of measuring the relative orientation scales with the strength of the CSA interaction, described by the anisotropy parameter δ.

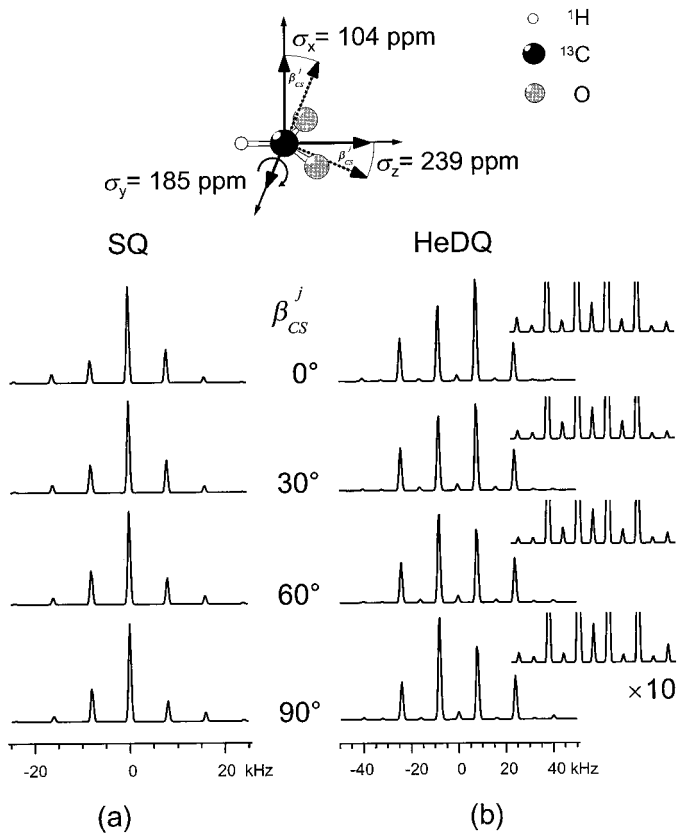

FIG. 3. Calculated dipolar (a) ^{13}C SQ and (b) HeDQ spinning-sideband patterns for a ^{13}C–^{1}H spin pair at 8 kHz MAS, showing the effect of ^{13}C chemical-shift anisotropy on the patterns. The patterns depend on the relative orientation of the dipolar and the CSA tensor, which is here represented by varying the β^j_{CS} Euler angle, corresponding to a rotation of the CSA tensor around the *y* axis of the molecular frame. In the case of HeDQ (b), even-order sidebands and a centerband arise, containing additional information on the magnitude and orientation of the CSA tensor (see inset). The CSA tensor principal values used here were those of calcium formate (*33*), and the distance r_{CH} was set to 115 pm (best fit distance for the experimental HeDQ spectra; see below). The spectra are plotted on the same vertical scale.

The influence of remote protons on HeDQ spinning-sideband patterns has been studied by numerically solving the Liouville–von Neumann equation for a three-spin system. To this end, a C++ program has been developed, which performs discrete step-by-step evaluations of the propagators corresponding to the pulse sequence to be simulated. The simulation time step is usually 1 μs, and CSA and all dipolar interactions are taken into account. The powder averaging procedure is again performed using the same REPULSION method described above. In the simulation program, perfect coherence selection is achieved by simply setting all elements of the density matrix to zero except for those corresponding to heteronuclear DQ coherences.

In Fig. 4, spectra for two possible arrangements of the three spins (one ^{13}C–^{1}H spin pair of the formate and an additional

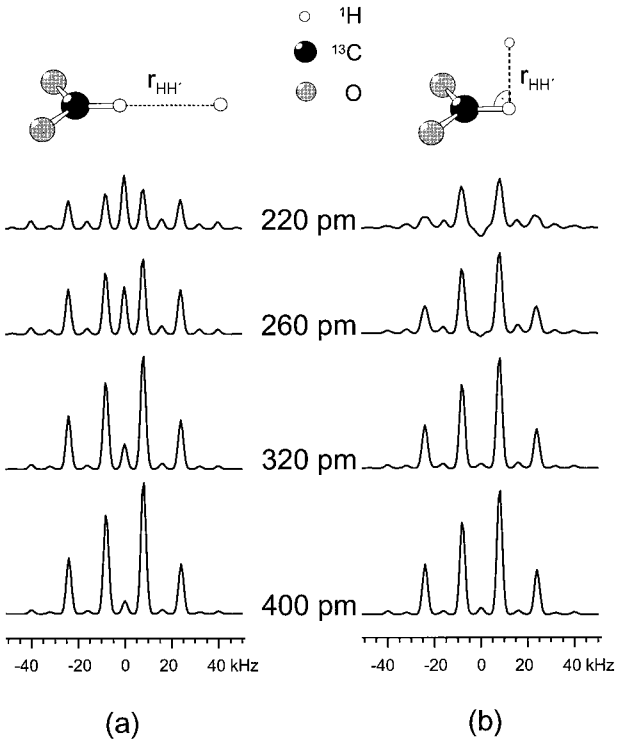

FIG. 4. Simulated dipolar HeDQ spinning-sideband patterns for a ^{13}C–^{1}H spin pair at 8 kHz MAS. The effect of an additional remote proton on the patterns is shown. In (a), all three spins are arranged linearly (C–H$\cdots$H′), whereas in (b) the remote proton is located above the formate proton, perpendicular to the formate plane. The CSA of the formate carbon was taken into account, and the distance r_{CH} was set to 115 pm. All spectra are plotted on the same vertical scale.

remote proton) are compared. In the case of the linear arrangement, the interactions present in t_1 are still inhomogeneous in nature (therefore the signal is periodic with respect to τ_R; see Ref. (*29*, p. 132)). Upon decreasing the distance between the third spin and the pair, a decrease in overall signal intensity and the appearance of a strong centerband and even-order spinning sidebands are observed (Fig. 4a). For a remote proton located above (or below) the formate proton, the proton–proton vector being perpendicular to the formate plane, phase distortions and homogeneous broadening of the signals are observed (Fig. 4b). In the latter case, the dipolar coupling of ^{1}H′ with the ^{13}C–^{1}H spin pair is different compared to the linear topology, leading to different HeDQ patterns for short distances $r_{HH'}$. This is a true geometrical effect, since the contribution of the ^{13}C–remote proton coupling is in both cases small.

The signal reduction is due to the relatively strong perturbing homonuclear interaction between the two protons compared with the heteronuclear ^{13}C–^{1}H dipolar coupling, which leads to dephasing of the signal during excitation/reconversion. The observation of a centerband and even-order sidebands is a general feature of MQ spectroscopy for cases where the coherence evolving in t_1 is not the total spin coherence, so that sidebands do not arise only due to reconversion rotor encoding (the mechanism considered under Theory), but also due to evolution rotor modulation; i.e., the presence of additional (dipolar) interactions influence the MQ coherence evolution during t_1. These mechanisms of MQ sideband generation have been analyzed in detail for the equivalent case of quadrupolar systems (*12*). The appearance of these *additional* spinning sidebands is therefore a good measure of the extent to which the use of the spin-pair approximation for the evaluation of the dipolar coupling is justified. In comparison, for the case of SQ patterns, such information is less apparent, being obtained only from the linewidths of the spinning sidebands.

Further investigations have shown that all these adverse effects can be reduced to a great extent by increasing the spinning speed (it is then however necessary to use recoupling sequences) and introducing homonuclear decoupling of the protons. Further work along these lines is under way. For a successful application of heteronuclear DQ spectroscopy involving protons in a strongly coupled spin network, as commonly encountered in most organic solids, it is especially important to be aware of these complications.

EXPERIMENTAL

Samples

Deuterated ammonium formate was chosen as a model substance for an isolated ^{13}C–^{1}H spin pair due to its favorable spin–lattice relaxation behavior, and the possibility of studying the effect of remote protons by comparison to measurements of undeuterated formate. The widely used calcium formate was not employed in this work because the presence of paramagnetic doping agents such as Mn^{2+} or Fe^{3+}—which are essential for achieving an experimentally tolerable T_1 value—was found to cause distortions in the DQ spinning-sideband patterns and therefore hamper an exact evaluation of the dipolar coupling constants.

Deuteration was performed by dissolving ammonium formate (NH_4HCO_2) in D_2O (about one percent by weight formate), gently heating to about 80°C, and evaporating the D_2O at this temperature under reduced pressure. This procedure was repeated twice. The crystals were then immediately dried at 80°C in an oil pump vacuum for about 20 min. Long exposure to vacuum must be avoided because of loss of the formate due to its high vapor pressure. Ammonium formate is highly hygroscopic, and thus the rotor was filled in a glove box to avoid reexchange of water protons. We estimate the degree of deuteration to be about 95%. The T_1 relaxation times of the ammonium formates are strongly dependent on the degree of deuteration, such that recycle times were 0.5 and 5 s for the undeuterated and the deuterated formate, respectively.

For the dipolar connectivity measurements, bisphenol A polycarbonate, henceforth referred to as polycarbonate (PC), was chosen as a typical amorphous polymer with a large dispersion of ^{13}C chemical shifts. The polymer was melted

directly into the rotor to achieve the optimum filling. The T_1 relaxation time of PC is relatively short, allowing recycle times of only 1.5 s.

Instrumentation

All experiments were performed on a Bruker DSX 300 spectrometer operating at 300.23 MHz for ^{1}H and 75.49 MHz for ^{13}C. A commercial Bruker double-resonance MAS probe supporting rotors of diameter 4 mm was used. To avoid problems with B_1 inhomogeneity, the samples were all located in the middle part of the rotor using Teflon spacers. The 90° pulse length was 3 μs, corresponding to a B_1 radiofrequency magnetic field strength of $\omega_1/2\pi = 83.3$ kHz. Continuous wave dipolar decoupling, $\omega_1/2\pi \approx 65$ kHz, was applied in all ^{13}C measurements during acquisition.

Pulse Sequences

Heteronuclear DQ spinning-sideband patterns were measured in 2D experiments following the pulse scheme in Fig. 1. The HeDQ coherences excitation was preceded by a conventional Hartmann–Hahn cross-polarization (CP) sequence with a proton B_1 field corresponding to $\omega_1/2\pi = 83.3$ kHz and the ^{13}C field matched on the first rotational sideband (83.3 kHz $-$ ν_R). CP contact times were chosen to achieve maximum signal, corresponding to 100 and 500 μs for the formate and PC samples, respectively. Using 90^0 flip-back pulses on both channels, initial z magnetization was created for both spin species. The relative magnitude of I and S magnetization could be estimated (by leaving out the flip-back pulses in the preparation period for either channel and observing the loss in signal) to be about the same, corresponding to equal coefficients p_S and p_I in Eqs. [15] and [16]. These values were used in all simulations as well, but it should be noted that the dependence of the sideband intensities on the relative distribution of magnetization within experimental imperfections, like matching of the CP field strengths, is rather small. Simulations showed that a relative variation of the coefficients of 50% amounted to intensity changes of not more than about $\pm$3% for the case of the relatively large CSA contribution during excitation of a ^{13}C in formate. Larger effects could be expected if the other spin (^{1}H in our case) had a nonnegligible CSA, e.g., ^{15}N or ^{31}P.

To select the HeDQ coherences, the phases of all pulses in the excitation period (both channels) were cycled simultaneously in four steps of 90° increments, together with a 180° phase change of the readout pulse for each step. Additionally, CYCLOPS together with a two-step cycle to correct for flip-angle deviations (all excitation and reconversion pulses shifted by 180°, keeping the phase of the read-out pulse constant) was added, yielding a 32-step phase cycle. The dephasing delays t_d were on the order of 10 ms, which does not lead to significant signal reduction due to the comparably long ^{13}C T_1 relaxation times, and ensures almost complete relaxation of unwanted coherences. For nuclei with short T_1, a long purging delay can

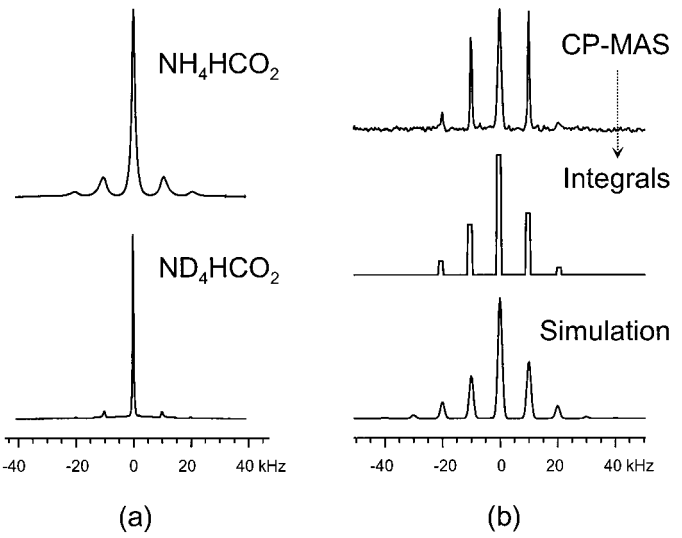

FIG. 5. Spectra characterizing the formate samples used for the HeDQ measuments: In (a), ^{1}H SQ MAS ($\nu_R = 10$ kHz) spectra are compared for the deuterated and undeuterated ammonium formate samples. In (b), the relative sideband intensities obtained by integration from a ^{13}C CP MAS spectrum without ^{1}H decoupling at 10 kHz MAS of ND_4HCO_2 are shown to fit a calculated heteronuclear dipolar sideband pattern (Eq. [17]) including CSA with a distance of $r_{CH} = 110$ pm.

easily be avoided by an additional phase cycle of the z filter. To achieve sign discrimination in the F_1 dimension, the TPPI method extended for DQ spectroscopy was used; i.e., the phase of either excitation or reconversion is incremented by 45° for subsequent slices. Typically, 128 slices in t_1 with increments of 3.5 to 6 μs were measured, corresponding to between two and five rotor periods of acquisition in t_1 and a total experiment time of 24 to 36 h for each HeDQ spectrum of PC or deuterated formate, with ^{13}C in natural abundance. Due to its fast T_1 relaxation, and thus short repetition time (0.5 s for the undeuterated and 5 s for the deuterated formate), spectra of the undeuterated ammonium formate were acquired in typically 8–12 h.

Due to the large spread of chemical shifts in PC, which is a polymer containing both aliphatic and aromatic groups, the offset-compensated version of the five-pulse sequence (Fig. 1b) had to be used. Offset compensation is of great importance for nuclei with a large dispersion of chemical shifts, such as ^{13}C, where it is necessary to achieve uniform excitation over a spectral width in the order of 15 kHz. Otherwise, for the usual spectral range of ^{13}C, the DQ excitation efficiency for signals far from resonance would be almost zero. The theoretical derivation did not take into account the π pulses in the middle of the excitation and reconversion intervals. It may merely be mentioned that the incomplete refocusing of the CSA evolution within $\tau_R/2$ (only possible within 2 τ_R) adds some small *phase distortions* to the spinning-sideband patterns, which are however hardly visible experimentally. Moreover, such slight phase errors are tolerable as long as only connectivities are to be determined.

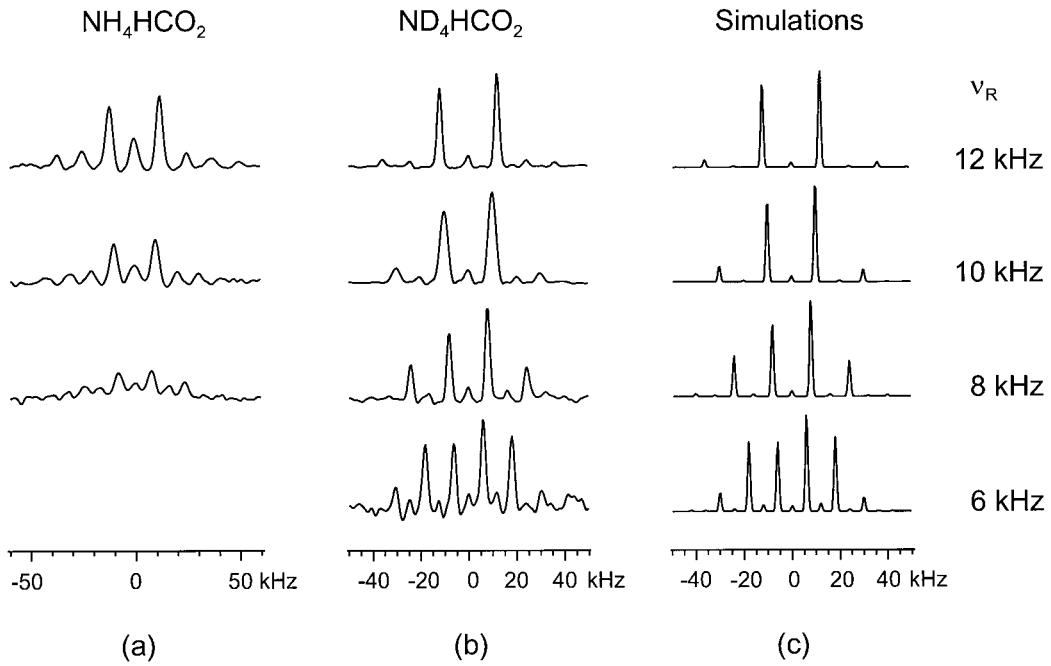

FIG. 6. Heteronuclear ^{13}C-detected DQ spinning-sideband patterns for (a) undeuterated and (b) deuterated ammonium formate at different spinning frequencies. The spectra represent sum projections of the ω_1 dimension of two-dimensional experiments corresponding to the experimental scheme in Fig. 1. Only weak Gaussian broadening was applied to the spectra in (a), which, for comparison of the intensities, are also plotted on the same vertical scale. In contrast, a relatively large damping function had to be applied in (b) in order to avoid cutoff effects, and the line broadening is 2 kHz, except for the spectrum at 10 kHz MAS, which is broadened by 3.5 kHz due to a smaller number of acquired t_1 slices. These spectra were then scaled to equal peak heights. The experimental results for ND_4HCO_2 are compared to (c) spectra calculated using Eqs. [15] and [16], with the CSA values given in Fig. 3, and an orientation of the CSA tensor colinear with the dipolar tensor ($\beta_{CS}^{S} = 0$).

RESULTS AND DISCUSSION

HeDQ Spinning-Sideband Patterns for ^{1}H–^{13}C Pairs

The degree of isolation of the ^{1}H–^{13}C spin pair achieved by deuteration was tested in different experiments. These results are presented in Fig. 5. ^{1}H SQ MAS spectra of deuterated and undeuterated formate at a rotor frequency of 10 kHz are shown in Fig. 5a. The almost complete disappearance of dipolar spinning sidebands and the marked line narrowing for ND_4HCO_2 illustrate the clear suppression of homonuclear ^{1}H–^{1}H dipolar interactions. The good isolation of the spin pair allowed us to measure a heteronuclear SQ dipolar spinning-sideband pattern of ^{13}C by simply omitting continuous wave dipolar decoupling during the acquisition interval in a CP MAS experiment (see Fig. 5b). Due to reasons not completely understood, the linewidths were different for different sideband orders. Therefore, the integrals of the peaks are compared with intensities from a simulation performed within the two-spin approximation including CSA (Eqs. [16] and [17]). A C–H distance of 110 pm gave the best fit to the experimental spectrum. This result means that the rigid heteronuclear spin-pair approximation used in the above theoretical derivations is applicable to the ND_4HCO_2 system.

Experimental ^{13}C-detected HeDQ spinning-sideband patterns obtained for the formates, along with simulated patterns, are depicted in Fig. 6. The most important conclusions can be drawn by comparing the experimental results obtained for the two types of formate: Spectra of NH_4HCO_2 exhibit pronounced centerbands and even-order spinning sidebands, along with fairly low S/N ratios. A rather large perturbing influence is thus exerted by the abundant proton background in the undeuterated formate, although from the crystal structure (*34*), the closest formate proton–remote proton distance is derived to be 280 pm, which gives a dipolar proton–proton interaction more than five times smaller than the C–H interaction, not even considering the motional averaging due to rapid tumbling of the NH_4^+ ions. As predicted by the comparably simplistic three-spin calculations (see Fig. 4), the signal-to-noise ratio is markedly reduced if couplings to remote protons are present. In addition, we believe that this is also due to fast relaxation of the antiphase magnetizations evolving in the excitation/reconversion intervals. Likewise, the HeDQ coherence during t_1 relaxes comparably fast, which leads to broad lines; very little line broadening was applied in the NH_4HCO_2 spectra, whereas the line broadening in the ND_4HCO_2 is mostly artificial in order to avoid cutoff effects in the indirect dimension. As is obvious from the DQ FIDs for the two samples at $\nu_R = 12$ kHz (Fig. 7), the HeDQ signal of ND_4HCO_2 was not fully relaxed after five rotor periods of t_1 evolution. In the undeuterated case, almost no signal was detectable after three rotor periods.

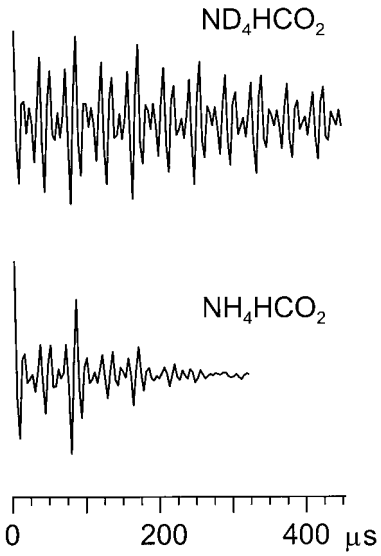

FIG. 7. Sum-projected DQ time domain signals of the HeDQ coherences during t_1 at $\nu_R = 12$ kHz, illustrating the different relaxation behavior of these coherences in the two formates. Fourier transformation yields the corresponding spectra in Fig. 6.

As already concluded from computer simulations, a remedy to this problem is homonuclear decoupling during t_1 and even during excitation/reconversion. Experiments along these lines are currently under way. Under increasingly fast MAS, the *S*/*N* also increases considerably, which is a result of the spinning out of interactions responsible for relaxation of the MQ coherences.

The third column in Fig. 6 shows simulated HeDQ patterns calculated using the theoretical spin-pair formulae (Eqs. [15] and [16]). With a distance $r_{CH} = 115\ (\pm 5)$ pm, the simulations match the experimental data best. From crystallographic measurements, C–H bond lengths are typically of the order of 110 pm. Nevertheless, the result agrees with earlier findings (*35*, and references therein), which show that distances measured by NMR are expected to be slightly larger than those from scattering experiments due to different averaging of fast vibrational motions of the molecules.

The simulations assuming the expected colinear arrangement of the dipolar and the CS tensor with σ_z along the dipolar axis gave the best match, although it should be stated that the dependence of the patterns on the orientation of the tensors is rather weak (but still larger than for SQ spectra). An accurate determination of the angles α_{CS}^j and β_{CS}^j would require better experimental data, for example, as would be provided by isotopic labeling. Also, the even-order spinning sidebands are slightly more pronounced in the experimental spectra, indicating a small residual influence of remote protons, probably from incomplete deuteration.

Dipolar Connectivities Using HeDQ Spectra

A full two-dimensional HeDQ spectrum of polycarbonate is presented in Fig. 8. As is obvious from the spectrum, by virtue of the presence of the refocusing π pulses in the compensated variant of the experiment, the excitation efficiency is not dependent on the frequency offset, which is here located in the middle of the spectrum. The expected coupling of the aliphatic carbons (a, b) to the aliphatic protons and the couplings of the aromatic carbons (c, d, e) to the aromatic protons can clearly be

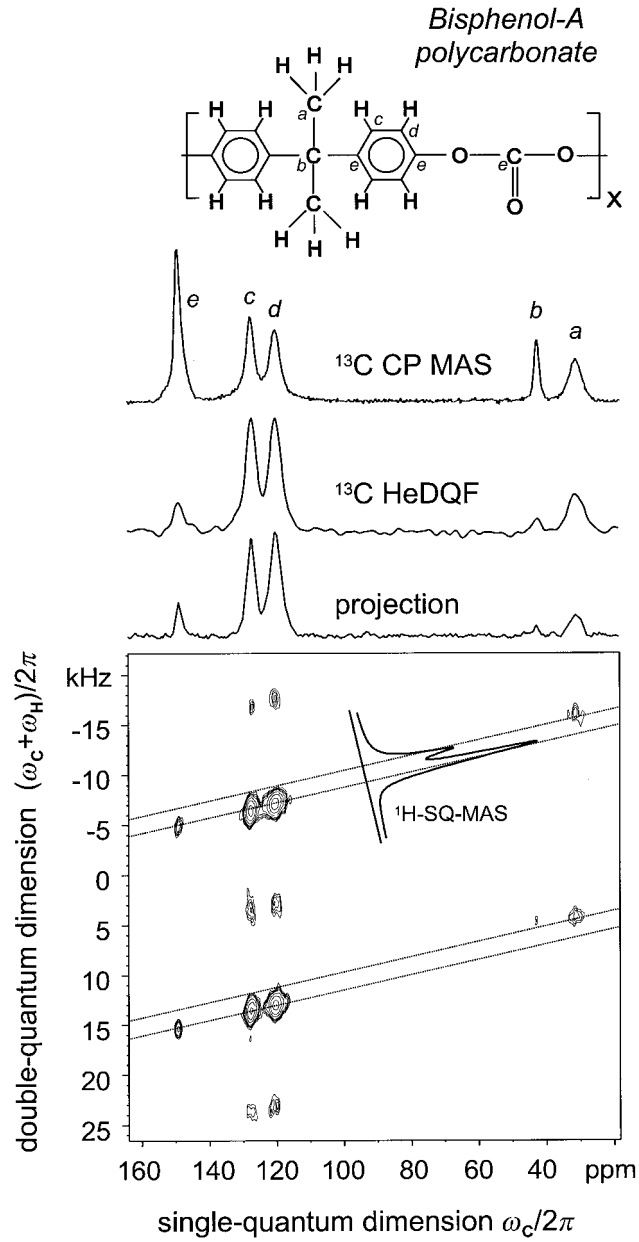

FIG. 8. Two-dimensional ^{13}C-detected HeDQ spectrum of polycarbonate, recorded at a MAS frequency of 10 kHz, using the compensated variant of the pulse sequence in Fig. 1. The projection along the DQ dimension is compared with a HeDQ-filtered spectrum (which corresponds to the Fourier transform of the first slice) and a conventional ^{13}C CP MAS spectrum. The relative proton shifts in the DQ dimension can be evaluated by projecting the spectrum along the $\omega_C + \omega_H = \omega_C$ diagonal, and are shown to be in accord with those from a ^{1}H SQ MAS spectrum.

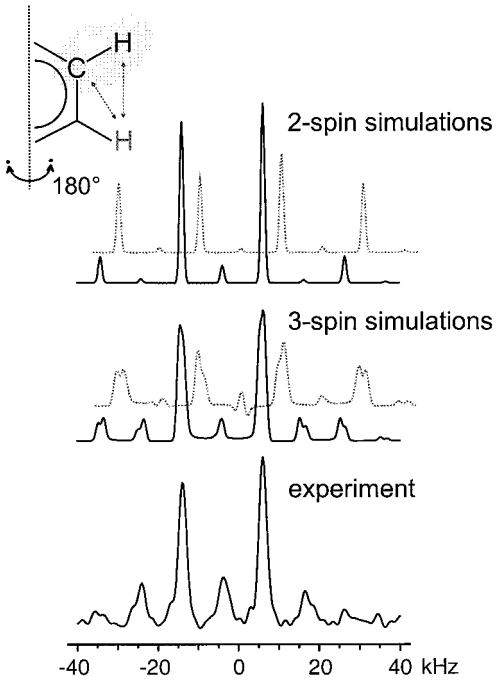

FIG. 9. Sum projection of one of the aromatic signals (d) in the HeDQ spectrum of PC (cf. Fig. 8) along the DQ dimension (bottom trace). The experimental spectrum is compared with spin-pair simulations (top trace) and another pair of simulations (middle trace), taking the influence of the neighboring aromatic proton into account. The simulations include ^{13}C CSA and correspond to the inclusion (solid lines) or absence (dashed lines) of a fast 180° flip motion. The simulations with and without the ring flip are plotted on the same vertical scale.

identified. No cross couplings between, e.g., methyl protons and aromatic carbons are visible. Thus the method is sensitive to only the strongest couplings in the system. Weaker couplings to the quaternary carbons (b, e) in the system are still visible, but with the signal exclusively present in the first-order sidebands. By simply measuring a heteronuclear double-quantum-filtered spectrum (which corresponds to the first slice, with $t_1 = 0$, in the 2D experiment), it is possible to obtain a crude estimate of the heteronuclear coupling constants, i.e., to distinguish carbons directly bound to protons from quaternary ones. At 10 kHz MAS, the resolution in the DQ dimension is comparable to the resolution of the ^{1}H SQ MAS spectrum, such that a further increase of the rotor frequency and homonuclear decoupling during t_1 evolution would be needed to increase the information content of HeDQ spectra. Yet the pulse sequence presented here is limited to strong couplings, such that at MAS frequencies larger than 20 kHz even the signals of directly bound ^{1}H–^{13}C pairs become considerably weakened. For very fast MAS up to 35 kHz, or in the case of HeDQ coherences involving nuclei with small gyromagnetic ratios, efficient recoupling techniques are required.

Finally, in Fig. 9, the sum projection of the HeDQ signal of one of the aromatic carbons (d), along with simulated patterns, is displayed. The spinning-sideband pattern exhibits a relatively strong centerband and second-order sidebands, as is to be expected from the abundant proton network found in organic solids. Nevertheless, some features of the spectrum can be understood by considering the fact that the phenyl ring performs a fast 180° flip motion around the axis defined by the polymer backbone. This motion leaves two protons and one ^{13}C as a relatively isolated three-spin system (*36*). In Fig. 9, the measured HeDQ pattern for this ^{13}C is compared with two-spin and full three-spin simulations of the phenyl ring in bisphenol A including CSA (*37*) and bond distances from crystallographic measurements (increased by 5% to account for different motional averaging) on bisphenol A pivaloate (*38*), with and without fast 180° flips. The effects considered in the three-spin simulation including the flips cannot fully account for the features of the experimental spectrum, but, by comparing this simulation with the one not taking into account the flips, it is obvious that the partial averaging due to the *motional process* accounts for a substantial spectral simplification, and a gain in signal intensity due to the suppression of perturbing couplings.

CONCLUSIONS AND OUTLOOK

A new pulse sequence for exciting double-quantum coherences in rigid heteronuclear spin systems has been introduced, and it has been shown that high resolution and sensitivity are provided by fast MAS. The sequence allows the measurement of dipolar spinning-sideband patterns originating from HeDQ coherences. The general features of such patterns for the case of isolated spin-$\frac{1}{2}$ pairs have been investigated both theoretically and experimentally. It has been demonstrated that the chemical shielding interactions of both spin species affect the HeDQ patterns and consequently, the relative orientation of the CSA tensor relative to the dipolar tensor can in principle be derived from such measurements. Compared to ^{13}C single-quantum spinning-sideband patterns, the effect of the chemical-shift interaction is *enhanced* in the HeDQ patterns due to rotor modulation of this interaction during the *excitation, evolution,* and *reconversion* periods of the experiment. For the case of preparation/reconversion time $\tau = \tau_R/2$ and isolated IS spin pairs, the chemical-shift interactions lead to properly phased, asymmetric HeDQ patterns with low-intensity even-order spinning sidebands.

HeDQ patterns can be recorded using recoupling (*20, 21*) as well as pulse sequences employing the quasi-static excitation method. The sequence introduced in this work is a new quasi-static method for the excitation of heteronuclear multiple-quantum coherences under MAS. It is based on the five-pulse sequence applied synchronously at the resonance frequencies of both heteronuclei. The SYNCHRON4 pulse sequence is robust and has the advantage of simplicity. The symmetric design of the sequence with respect to the two channels opens up the possibility of using different preparation schemes and I-

or S-spin detection, as a means of achieving different encoding of the patterns by the chemical shielding interaction of the different nuclei during the excitation or reconversion periods. A broadband excitation of HeDQ coherences can be achieved by 180° refocusing pulses applied in the middle of the excitation and reconversion periods.

High-resolution HeDQ MAS NMR spectroscopy has also been shown to be applicable to probing heteronuclear dipolar proximities in organic solids with ^{13}C in *natural abundance*. As is evident from the HeDQ spinning-sideband patterns visible in a two-dimensional HeDQ spectrum of a sample of polycarbonate, sideband analysis is limited to well-isolated spin pairs unperturbed by remote spins. In the fast spinning limit, it is nevertheless possible to extract valuable information on the relative dipolar couplings, thus distances, between the nuclei involved. Still, due to the quasi-static character of the HeDQ excitation, the method presented is limited to strong couplings; a further problem being that for reduced MAS frequencies (needed to probe weaker couplings) S/N decreases due to relaxation of the signals during excitation/reconversion.

As already mentioned, a remedy to these problems is very fast MAS ($\nu_R > 20$ kHz), combined with the use of recoupling techniques. The influence of remote spins, which affect the MQ relaxation (thus S/N) and cause distortions in the sideband patterns, can be expected to be significantly decreased at such high spinning frequencies. Also, homonuclear decoupling during t_1 will increase the resolution of ^{13}C–^{1}H correlation experiments. New developments along these lines will soon be published elsewhere. One could also envisage a multidimensional experiment establishing, for instance, ^{1}H–^{1}H and ^{13}C–^{1}H chemical-shift correlations, which may accurately be discriminated by different dipolar coupling strengths between the nuclei. As to advanced solid-state structure determination, we believe that HeDQ techniques involving coherent polarization transfer will be the methods of choice rather than incoherent ZQ techniques (e.g., CP correlation), due to the much more localized, and as regards quantitative interpretation, less demanding character of two-spin modes such as HeDQ. We believe that heteronuclear MQ MAS NMR spectroscopy will open up new perspectives, especially with respect to site selectivity and resolution, which are the prime prerequisites for NMR structure determination of complex systems, such as polymers or biomolecules in the solid state.

APPENDIX

Expressions for the time dependence of the dipolar coupling (Eq. [4]) and the chemical-shift evolution (Eq. [10]) under MAS were given under Theory. In the dipolar case, the symmetry axis of the interaction tensor is orientated along the z direction. Here, we give expressions for the coefficients C_1, C_2, S_1, and S_2 in Eq. [10] for arbitrary orientations of the CSA tensors with respect to the dipolar (z) axis. Since a general solution of Eq. [7] is algebraically demanding, we confine ourselves first to the case of a general, nondiagonal, arbitrarily oriented CSA tensor $\boldsymbol{\sigma}_{P_D}$ specified by its components σ_{ij} in the dipolar frame. The coefficients for the traceless symmetric part of the tensor read (*29*)

$$\begin{aligned} C_1 = \tfrac{2}{3}\sqrt{2}\{&\tfrac{1}{4}(\sigma_{11} + \sigma_{22} - 2\sigma_{33})\sin 2\beta_D^{IS} \\ &- \tfrac{1}{4}(\sigma_{22} - \sigma_{11})\sin 2\beta_D^{IS}\cos 2\alpha_D^{IS} \\ &+ \tfrac{1}{2}\sigma_{12}\sin 2\beta_D^{IS}\sin 2\alpha_D^{IS} + \sigma_{13}\cos 2\beta_D^{IS}\cos \alpha_D^{IS} \\ &+ \sigma_{23}\cos 2\beta_D^{IS}\sin \alpha_D^{IS}\}, \end{aligned} \quad [A1]$$

$$\begin{aligned} C_2 = \tfrac{1}{3}\{&\tfrac{1}{2}(-\sigma_{11} - \sigma_{22} + 2\sigma_{33})\sin^2\beta_D^{IS} \\ &- \tfrac{1}{2}(\sigma_{22} - \sigma_{11})(1 + \cos^2\beta_D^{IS})\cos 2\alpha \\ &+ \sigma_{12}(1 + \cos^2\beta_D^{IS})\sin 2\alpha_D^{IS} - \sigma_{13}\sin 2\beta_D^{IS}\cos \alpha_D^{IS} \\ &- \sigma_{23}\sin 2\beta_D^{IS}\sin \alpha_D^{IS}\}, \end{aligned} \quad [A2]$$

$$\begin{aligned} S_1 = \tfrac{2}{3}\sqrt{2}\{&\tfrac{1}{2}(\sigma_{22} - \sigma_{11})\sin \beta_D^{IS}\sin 2\alpha_D^{IS} \\ &+ \sigma_{12}\sin \beta_D^{IS}\cos 2\alpha_D^{IS} - \sigma_{13}\cos \beta_D^{IS}\sin \alpha_D^{IS} \\ &+ \sigma_{23}\cos \beta_D^{IS}\cos \alpha_D^{IS}\}, \end{aligned} \quad [A3]$$

$$\begin{aligned} S_2 = \tfrac{2}{3}\{&\tfrac{1}{2}(\sigma_{22} - \sigma_{11})\cos \beta_D^{IS}\sin 2\alpha_D^{IS} \\ &+ \sigma_{12}\cos \beta_D^{IS}\cos 2\alpha_D^{IS} + \sigma_{13}\sin \beta_D^{IS}\sin \alpha_D^{IS} \\ &- \sigma_{23}\sin \beta_D^{IS}\cos \alpha_D^{IS}\}, \end{aligned} \quad [A4]$$

where (α_D^{IS}, β_D^{IS}) are Euler angles relating the molecular (i.e., dipolar) frame to the rotor system, within which the powder average must be performed. The traceless symmetric part of a CSA tensor in its principal axis frame reads

$$\begin{aligned} \boldsymbol{\sigma}_{P_{CS}} &= \begin{pmatrix} (\sigma_x - \sigma_{iso}) & 0 & 0 \\ 0 & (\sigma_y - \sigma_{iso}) & 0 \\ 0 & 0 & (\sigma_z - \sigma_{iso}) \end{pmatrix} \\ &= -\frac{\delta}{\omega_0}\cdot\begin{pmatrix} -\tfrac{1}{2}(1+\eta) & 0 & 0 \\ 0 & -\tfrac{1}{2}(1-\eta) & 0 \\ 0 & 0 & 1 \end{pmatrix}. \end{aligned} \quad [A5]$$

The transition from the principal axis frame of the tensor to the dipolar frame is most straightforwardly performed by matrix multiplication

$$\boldsymbol{\sigma}_{P_D} = \tilde{\mathbf{R}}_{P_{CS}P_D}\boldsymbol{\sigma}_{P_{CS}}\tilde{\mathbf{R}}^{-1}_{P_{CS}P_D}, \quad [A6]$$

where

$$\tilde{\mathbf{R}}_{P_{CS}P_D} = \begin{pmatrix} \cos\alpha^j_{CS}\cos\beta^j_{CS}\cos\gamma^j_{CS} - \sin\alpha^j_{CS}\sin\gamma^j_{CS} & \sin\alpha^j_{CS}\cos\beta^j_{CS}\cos\gamma^j_{CS} + \cos\alpha^j_{CS}\sin\gamma^j_{CS} & -\sin\beta^j_{CS}\cos\gamma^j_{CS} \\ -\cos\alpha^j_{CS}\cos\beta^j_{CS}\sin\gamma^j_{CS} - \sin\alpha^j_{CS}\cos\gamma^j_{CS} & -\sin\alpha^j_{CS}\cos\beta^j_{CS}\sin\gamma^j_{CS} + \cos\alpha^j_{CS}\cos\gamma^j_{CS} & \sin\beta^j_{CS}\sin\gamma^j_{CS} \\ \cos\alpha^j_{CS}\sin\beta^j_{CS} & \sin\alpha^j_{CS}\sin\beta^j_{CS} & \cos\gamma^j_{CS} \end{pmatrix}$$
$$= (\tilde{\mathbf{R}}^{-1}_{P_{CS}P_D})^T. \qquad [A7]$$

$(\alpha^j_{CS}, \beta^j_{CS}, \gamma^j_{CS})$ are the Euler angles relating the CSA tensor in its principal axis frame to the molecular/dipolar frame. $\boldsymbol{\sigma}_{P_D}$ can be evaluated numerically from Eq. [A6] and its components can then be substituted into Eqs [A1]–[A4]. As to calculation efficiency, this is the method of choice for numerical evaluations of the time domain signals according to Eqs. [15]–[18], because the setup of the relative tensor orientations can be moved outside of the powder averaging loop.

For one special case, the algebra involved is still within acceptable range. If only one CSA tensor is considered, γ^j_{CS} is of no importance, since it is only when two CSA tensors are being correlated that, at least for one of the tensors, a final rotation around the dipolar z axis must be considered in order to fully describe the relative orientation of all three tensors in question. Since under Experimental of this paper only cases where $\sigma^I_{CS} = 0$ are considered, which is the case when dealing with the negligible CSA of spin I = ^{1}H, we here give the evaluation of the coefficients [A1]–[A4] for the case of $\gamma^S_{CS} = 0$. These equations, together with Eq. [10], represent the solution of Eq. [7] for this special case. We can finally write

$$C_1 = \frac{2\sqrt{2}}{3}\left\{\frac{\delta\eta}{2}\sin(\alpha^{IS}_D)\cos(2\beta^{IS}_D)\sin(2\alpha^j_{CS})\sin(\beta^j_{CS}) - \frac{\delta}{4}\cos(\alpha^{IS}_D)\cos(2\beta^{IS}_D)\sin(2\beta^j_{CS}) \times [\eta\cos(2\alpha^j_{CS}) + 3] - \frac{\delta\eta}{4}\sin(2\alpha^{IS}_D)\sin(2\beta^{IS}_D)\sin(2\alpha^j_{CS})\cos(\beta^j_{CS}) - \frac{\delta}{8}\cos(2\alpha^{IS}_D)\sin(2\beta^{IS}_D) \times [\eta\cos(2\alpha^j_{CS})(\cos^2(\beta^j_{CS}) + 1) - 3\sin^2(\beta^j_{CS})] + \frac{3\delta}{8}\sin(2\beta^{IS}_D)[\sin^2(\beta^j_{CS}) \times (\eta\cos(2\alpha^j_{CS}) + 3) - 2]\right\}, \qquad [A8]$$

$$C_2 = \frac{1}{3}\left\{\frac{\delta\eta}{2}\sin(2\alpha^{IS}_D)(\cos^2(\beta^{IS}_D) + 1)\sin(2\alpha^j_{CS})\cos^2(\beta^j_{CS}) + \frac{\delta}{4}\cos(\alpha^{IS}_D)\sin(2\beta^{IS}_D)\sin(2\beta^j_{CS})[\eta\cos(2\alpha^j_{CS}) + 3] - \frac{\delta\eta}{2}\sin(\alpha^{IS}_D)\sin(2\beta^{IS}_D)\sin(2\alpha^j_{CS})\cos(\beta^j_{CS}) - \frac{\delta}{4}\cos(2\alpha^{IS}_D)(\cos^2(\beta^{IS}_D) + 1) \times [\eta\cos(2\alpha^j_{CS})(\cos^2(\beta^j_{CS}) + 1) - 3\sin^2(\beta^j_{CS})] + \frac{3\delta}{4}\sin^2(\beta^{IS}_D)[2 - \sin^2(\beta^j_{CS}) \times (\eta\cos(2\alpha^j_{CS}) + 3)]\right\}, \qquad [A9]$$

$$S_1 = \frac{2\sqrt{2}}{3}\left\{\frac{\delta\eta}{2}\cos(2\alpha^{IS}_D)\sin(\beta^{IS}_D)\sin(2\alpha^j_{CS})\cos(\beta^j_{CS}) - \frac{\delta}{4}\sin(\alpha^{IS}_D)\cos(\beta^{IS}_D)\sin(2\beta^j_{CS})[\eta\cos(2\alpha^j_{CS}) + 3] + \frac{\delta\eta}{4}\cos(\alpha^{IS}_D)\cos(2\beta^{IS}_D)\sin(2\alpha^j_{CS})\sin(\beta^j_{CS}) - \frac{\delta}{4}\sin(2\alpha^{IS}_D)\sin(\beta^{IS}_D)[\eta\cos(2\alpha^j_{CS}) \times (\cos^2(\beta^j_{CS}) + 1) - 3\sin^2(\beta^j_{CS})]\right\}, \qquad [A10]$$

$$S_2 = \frac{2}{3}\left\{\frac{\delta\eta}{2}\cos(2\alpha^{IS}_D)\cos(\beta^{IS}_D)\sin(2\alpha^j_{CS})\cos(\beta^j_{CS}) + \frac{\delta}{4}\sin(2\alpha^{IS}_D)\cos(\beta^{IS}_D) \times [\eta\cos(2\alpha^j_{CS})(\cos^2(\beta^j_{CS}) + 1) - 3\sin^2(\beta^j_{CS})] - \frac{\delta\eta}{2}\cos(\alpha^{IS}_D)\sin(\beta^{IS}_D)\sin(2\alpha^j_{CS})\sin(\beta^j_{CS}) - \frac{\delta}{4}\sin(\alpha^{IS}_D)\sin(\beta^{IS}_D)\sin(2\beta^j_{CS}) \times [\eta\cos(2\alpha^j_{CS}) + 3]\right\}. \qquad [A11]$$

ACKNOWLEDGMENTS

D.E.D. thanks the Alexander von Humbold-Stiftung for a senior research award and Prof. Dr. Bernhard Blümich for stimulating discussions. Discussions with Steven P. Brown and Claudiu Filip are gratefully acknowledged. Financial support was provided by the Deutsche Forschungsgemeinschaft, SFB 262.

REFERENCES

1. R. R. Ernst, G. Bodenhausen, and A. Wokaun, "Principles of Nuclear Magnetic Resonance in One and Two Dimensions," Oxford Univ. Press, New York (1987).
2. D. P. Weitekamp, *Adv. Magn. Reson.* **11,** 111 (1983).
3. M. Munowitz and A. Pines, *Adv. Chem. Phys.* **66,** 1 (1987).
4. T. J. Norwood, *Progr. NMR Spectrosc.* **24,** 295 (1992).
5. O. W. Sørensen, M. Rance, and R. R. Ernst, *J. Magn. Reson.* **56,** 527 (1984).
6. L. Müller, *J. Am. Chem. Soc.* **101,** 4481 (1979).
7. A. Bax, R. H. Griffey, and B. L. Hawkins, *J. Magn. Reson.* **55,** 301 (1983).
8. H. Geen, J. J. Titman, J. Gottwald, and H. W. Spiess, *Chem. Phys. Lett.* **227,** 79 (1994).
9. J. Gottwald, D. E. Demco, R. Graf, and H. W. Spiess, *Chem. Phys. Lett.* **243,** 314 (1995).
10. R. Graf, A. Heuer, and H. W. Spiess, *Phys. Rev. Lett.* **80,** 5738 (1998).
11. R. Graf, D. E. Demco, S. Hafner, and H. W. Spiess, *Solid State Nucl. Magn. Reson.* **12,** 139 (1998).
12. U. Friedrich, I. Schnell, S. P. Brown, A. Lupulescu, D. E. Demco, and H. W. Spiess, *Mol. Phys.* **95,** 1209 (1998).
13. I. Schnell, S. Brown, H. Y. Lew, H. Ishida, and H. W. Spiess, *J. Am. Chem. Soc.* **120,** 11784 (1998).
14. R. Graf, D. E. Demco, J. Gottwald, S. Hafner, and H. W. Spiess, *J. Chem. Phys.* **106,** 885 (1997).
15. K. Schmidt-Rohr, *J. Magn. Reson.* **131,** 209 (1998).
16. X. Feng, Y. K. Lee, D. Standström, M. Edén, H. Maisel, A. Sebald, and M. H. Levitt, *Chem. Phys. Lett.* **257,** 314 (1996).
17. X. Feng, P. J. E. Verdegem, Y. K. Lee, D. Sandström, M. Edén, P. Bovee-Geurts, W. J. de Grip, J. Lugtenberg, H. J. M. de Groot, and M. H. Levitt, *J. Am. Chem. Soc.* **119,** 6853 (1997).
18. M. Feike, R. Graf, I. Schnell, C. Jäger, and H. W. Spiess, *J. Am. Chem. Soc.* **118,** 9631 (1996).
19. M. Feike, C. Jäger, and H. W. Spiess, *J. Non-Cryst. Solids* **223,** 200 (1998).
20. W. Sommer, J. Gottwald, D. E. Demco, and H. W. Spiess, *J. Magn. Reson. A* **113,** 131 (1995).
21. M. Hong, J. D. Gross, and R. G. Griffin, *J. Phys. Chem. B* **101,** 5869 (1997).
22. R. K. Hester, J. L. Ackerman, B. L. Neff, and J. W. Waugh, *Phys. Rev. Lett.* **36,** 1081 (1976).
23. M. Linder, A. Höhener, and R. R. Ernst, *J. Chem. Phys.* **73,** 4959 (1980).

23a. T. Nakai, J. Ashida, and T. Terao, *Mol. Phys.* **67,** 839 (1989).

24. M. G. Munowitz and R. G. Griffin, *J. Chem. Phys.* **76,** 2848 (1982).
25. T. Nakai, J. Ashida, and T. Terao, *J. Chem. Phys.* **88,** 6049 (1988).
26. T. Guillion and J. Schaefer, *J. Magn. Reson.* **81,** 196 (1989).
27. A. Bennett, R. G. Griffin, and S. Vega, *NMR Basic Princ. Prog.* **33,** 3 (1994).
28. D. Franke, C. Hudalla, and H. Eckert, *Solid State Nucl. Magn. Reson.* **1,** 33 (1992).
29. K. Schmidt-Rohr and H. W. Spiess, "Multi-dimensional Solid State NMR and Polymers," Academic Press, San Diego (1997).
30. H. W. Spiess, *NMR Basic Princ. Prog.* **15,** 55 (1978).
31. O. W. Sørensen, G. W. Eich, M. H. Levitt, G. Bodenhausen, and R. R. Ernst, *Prog. NMR Spectrosc.* **16,** 163 (1983).
32. M. Bak and N. Nielsen, *J. Magn. Reson.* **125,** 132 (1997).
33. J. L. Ackerman, J. Tegenfeldt, and J. S. Waugh, *J. Am. Chem. Soc.* **96,** 6843 (1974).
34. I. Nahringbauer, *Acta Crystallogr., Sect. B* **24,** 565 (1968).
35. T. Nakai, J. Ashida, and T. Terao, *Mol. Phys.* **67,** 839 (1989).
36. K. Schmidt-Rohr, J. Clauss, and H. W. Spiess, *Macromolecules* **25,** 3273 (1992).
37. A. K. Roy, A. A. Jones, and P. T. Inglefield, *Macromolecules* **19,** 1356 (1986).
38. D. Casarini, R. K. Harris, and A. M. Kenwright, *J. Mol. Struct.* **355,** 121 (1995).